Original Article

MOLECULAR METABOLISM

Salubrinal promotes phospho-eIF2α-dependent activation of UPR leading to autophagy-mediated attenuation of iron-induced insulin resistance

Khang Nguyen[1], Jialing Tang[1], Sungji Cho[1], Fan Ying[1], Hye Kyoung Sung[1], James Wonsuk Jahng[1], Kostas Pantopoulos[2], Gary Sweeney[1,*]

ABSTRACT

Identification of new mechanisms mediating insulin sensitivity is important to allow validation of corresponding therapeutic targets. In this study, we first used a cellular model of skeletal muscle cell iron overload and found that endoplasmic reticulum (ER) stress and insulin resistance occurred after iron treatment. Insulin sensitivity was assessed using cells engineered to express an Akt biosensor, based on nuclear FoxO localization, as well as western blotting for insulin signaling proteins. Use of salubrinal to elevate eIF2α phosphorylation and promote the unfolded protein response (UPR) attenuated iron-induced insulin resistance. Salubrinal induced autophagy flux and its beneficial effects on insulin sensitivity were not observed in autophagy-deficient cells generated by overexpressing a dominant-negative ATG5 mutant or via knockout of ATG7. This indicated the beneficial effect of salubrinal-induced UPR activation was autophagy-dependent. We translated these observations to an animal model of systemic iron overload-induced skeletal muscle insulin resistance where administration of salubrinal as pretreatment promoted eIF2α phosphorylation, enhanced autophagic flux in skeletal muscle and improved insulin responsiveness. Together, our results show that salubrinal elicited an eIF2α-autophagy axis leading to improved skeletal muscle insulin sensitivity both in vitro and in mice.

Keywords Insulin resistance; Iron; Autophagy; Endoplasmic reticulum

1. INTRODUCTION

Iron is an essential element that is involved in many biological processes and sustaining balanced iron levels are essential for preventing the onset of a number of diseases [1]. Existing studies on iron deficiency and iron overload have bolstered our understanding of the importance of iron homeostasis and its regulation [2]. From a clinical perspective, iron overload is also pathologically important in primary hemochromatosis and secondary iron-loading anemias including thalassemia and myelodysplastic syndromes [3–5]. Furthermore, iron overload is the culprit underlying some forms of cancer, inflammation, neurodegenerative diseases and, most significantly, cardiometabolic diseases [6–9].

Insulin resistance remains the most notable and consequential metabolic dysfunction [10]. Under this condition, cells and tissues do not respond well to insulin [11], with associated consequences of type 2 diabetes and heart failure [12–14]. The molecular mechanisms underlying insulin resistance are widespread, with autophagy and endoplasmic reticulum (ER) stress both known to be important [15–17]. Autophagy is a well conserved process of 'self-eating' involving degradation of cellular components such as damaged orgnelles and protein aggregates, thus playing important roles in maintaining cellular homeostasis [18]. Previous studies have established the significance of autophagy in regulating insulin signaling as well as metabolism in skeletal muscles [19]. By utilizing skeletal muscle cells, we previously showed that chronic iron overload leads to a profound autophagy defect via mTORC1-UVRAG inhibition that led to inhibition of autophagosome-lysosome reformation (ALR), with consequent insulin resistance [15].

In the endoplasmic reticulum, proteins are synthesized, modified, and transported to destined compartments. Perturbations in these processes can manifest as protein aggregation [20]. To survive a series of cellular stressors such as nutrient deficiency, Ca^{2+} imbalance, toxin and sustained oxidative stress [21–24] the unfolded protein response (UPR) will be engaged [25]. This can involve the activation of three transmembrane proteins: inositol-requiring protein 1 (IRE1), protein kinase RNA-like ER kinase (PERK) and activating transcription factor 6 (ATF6) [26]. These sensors aid in improving cellular homeostasis by expanding the ER protein-folding capacity, decreasing global mRNA translation and increasing ER-associated degradation (ERAD), among others [27]. Upon activation, PERK will phosphorylate the downstream eukaryotic translation initiation factor (eIF2α) at Ser51, which enhances translation of a subset of mRNAs, including that encoding the activating transcription factor 4 (ATF4) [28–30]. This enhances cellular homeostasis by inhibiting translation, facilitating amino acid synthesis, inducing antioxidative stress response genes and increasing expression of autophagy genes. However, connections between iron, ER

[1]Department of Biology, York University, Toronto, ON, Canada [2]Lady Davis Institute for Medical Research, Jewish General Hospital and Department of Medicine, McGill University, Montreal, Canada

*Corresponding author. Department of Biology, York University, 4700 Keele St, Toronto, M3J 1P3, Ontario, Canada. E-mail: gsweeney@yorku.ca (G. Sweeney).

Received December 8, 2023 • Revision received March 4, 2024 • Accepted March 15, 2024 • Available online 26 March 2024

https://doi.org/10.1016/j.molmet.2024.101921

stress, UPR induction and autophagy in the regulation of insulin resistance are not clearly understood.

In this study, we hypothesized that iron overload leads to ER stress with consequent UPR activation; yet simultaneous inhibition of autophagosome lysosome reformation (ALR) and autophagy flux precludes the ability of endogenous cellular control mechanisms to restore insulin sensitivity. The functional significance of autophagy was studied by using autophagy-deficient cell models generated via overexpressing a dominant-negative ATG5 mutant as well as via autophagy-knockout ATG7 cell line. The significance of observations in cellular models were translated to testing in an animal model of systemic iron overload.

2. MATERIALS AND METHODS

2.1. Cell culture and maintenance of L6 skeletal muscle cells

L6 rat skeletal muscle cell line was grown in alpha-minimum essential medium (AMEM) (Wisent; 210-010) containing 10% fetal bovine serum (FBS) (Wisent; 080-150) and 1% antibiotic/antimycotic (Gibco; 15240062) at 37 °C with 95% air and 5% CO_2. Cells were maintained in 75 cm^2 flasks and passed at 70% confluency. 3 mL of trypsin was first added to detach the cells from the flasks following by neutralization with 7 mL of 10% FBS AMEM. Cells were then centrifuged at 2000 RPM for 5 min. 5 mL of 10% FBS AMEM was added in the cells for resuspension, with 10% of total cell and media mix being used for further plating in the new flask. For iron treatment, Iron (II) sulfate heptahydrate (Sigma—Aldrich; 215422) was firstly prepared by dissolving in sterile distilled water with the stock concentration of 100 mM. Cells were then treated with iron treatment of $FeSO_4$ 250 μM in AMEM 0% FBS.

2.2. Western blotting for insulin signaling

L6 cells were seeded on 6 well plates until having 80—90% confluency. Cells were subjected to treatments of $FeSO_4$ 250 μM for 24-h followed by insulin 100 nM (Lilly; Humulin-R U-100) for 10 min. For salubrinal groups, cells were pretreated with salubrinal (Sigma Aldrich; SML0951) 30 μM for 30 min prior to iron treatment. For sephin1 (Sigma; SML1356) treatment, the concentration of 10 μM was treated in cells for 30 min prior to iron treatment. Samples were washed with PBS (Wisent; 311-010-CL) and prepared using lysis buffer. Cells were also syringed to ensure further lysis. The cells were then collected and centrifuged at 10,000 RPM for 5 min at 4 °C followed by denaturation at 95 °C for 5 min. Cell lysates were run on 8% SDS-PAGE gels conducted at 90 V for 2 h. The gels were transferred to a polyvinylidene difluoride (PVDF) membrane at 120 V for 1.5 h. Membranes were submerged in 3% bovine serum albumin (BSA) blocking buffer for 1 h, followed by overnight incubation in 1:1000 dilution of primary antibodies: phospho-Akt s473 (Cell Signaling; 9271) and phospho-ERK (Cell Signaling; 9106L) at 4 °C. Membranes were then washed with TBS-T three times before 1 h of secondary antibody incubation at room temperature. The secondary antibodies used was an anti-rabbit immunoglobulin G horseradish peroxidase-conjugated antibody (Cell Signaling; 7074) and anti-mouse antibody (Cell Signaling; 7076) at 1:5000 dilution. Membranes were then quickly washed with Clarity Western ECL Substrate solution and visualized using X-ray film development techniques. Western blot band intensity was quantified using ImageJ software, normalized to glyceraldehyde 3-phosphate dehydrogenase (GAPDH) (Cell Signaling; 2118) or total Akt (Cell Signaling; 9272).

For assessing the role of iron and salubrinal in activating UPR, L6 cells were seeded on 6 well plates until having 80—90% confluency. 4 groups of treatment were performed including control, salubrinal, iron and salubrinal iron. For control samples, cells were starved in AMEM media 0% FBS for 24 h. For iron-treated samples, cells were subjected to treatments of $FeSO_4$ 250 μM for 24 h. For salubrinal groups, cells were treated with salubrinal 30 μM for 30 min prior to iron treatment. Western blot analysis was performed according to protocol aforementioned. 2 primary antibodies were used in this assay including p-eIF2α (Cell Signaling; 9721) and ATF4 (Cell Signaling; 11815).

To assess the role of autophagy in beneficial effects of salubrinal: empty vector (EV), WT L6, ATG5K and ATG7 cells were seeded on 6 well plates until having 80—90% confluency. 4 treatment groups were determined including insulin, iron insulin, salubrinal insulin and salubrinal iron insulin. Cells were subjected to treatments of $FeSO_4$ 250 μM in AMEM 0% FBS for 24 h. For salubrinal groups, cells were pretreated with salubrinal 30 μM for 30 min prior to iron treatment. All treatments were followed by insulin 100 nM stimulation for 10 min. For Tat-beclin 1 (Novus Biologicals; NBP249888) treatment, the concentration of 5 μM was treated in cells for 24 h prior to iron treatment. Western blot analysis was performed according to protocol aforementioned.

2.3. Transforming *Escherichia coli* DH5α cells with SB100X and FoxO1 biosensor plasmids

50 ng circular DNA of FoxO1 (AddGene; 106278) and SB100X (AddGene; 34879) plasmids were thawed, added to competent *E. coli* DH5α cells and gently mixed. The tube with DNA and competent cells was placed in 42 °C waterbath for 1 min and transferred onto ice for 2 min to reduce damage to cells. 800 μL of Luria—Bertani (LB) broth (Invitrogen; 12795027) was prepared and added to the tube, then incubated for 1 h at 37 °C with 250 RPM shaking. Resulting bacterial cultures were spread on LB agar plates containing ampicillin and chloramphenicol (Sigma) for FoxO1 and SB100X plasmids, respectively. Plates were incubated inverted overnight at 37 °C. A colony was then selected after 12 h to be propagated further in LB broth with antibiotics for overnight shaking at 250 RPM and 37 °C.

2.4. Plasmid purification

125 mL of transformed bacterial culture was centrifuged for 20 min at 4,000× *g*. Pellets were resuspended using the buffers provided by the Invitrogen PureLink Fast Low-Endotoxin Midi Plasmid Purification Kit (Invitrogen; A35892). All purification steps were performed according to the protocol provided in the kit in order to elute plasmid products.

2.5. Sleeping beauty transfection of FoxO1 and biosensor plasmids into L6 skeletal muscle cells

Prior to transfection, low passage WT-L6 cells were cultured in a T75 flask to 90% confluency. 2 transfection mixtures were prepared. An integrase/DNA/OptiMEM mix was first created by adding FoxO1 Biosensor and SB100X plasmids at a 10:1 ratio respectively to OptiMEM (ThermoFisher; 31985062) for a total volume of 150 μL. The first mixture was then combined with the second tube containing 3.6 μL of Lipofectamine 2000 (Invitrogen; 11668019) and 146.4 μL of OptiMEM. The mixture was then vortexed for 2 s, spun down on tabletop centrifuge and incubated for 15 min at room temperature. On the other hand, L6 cells were trypsinized at room temperature for 15 min in order for the cells to detach from the bottom. The cells were then neutralized by adding AMEM media containing 10% FBS and antibiotics. 900 μL of cell and media mixture was seeded into 1-3 wells of a 6-well plate per plasmid. 100 μL of DNA and lipofectamine mix was then added in each well. Plate was gently shook to mix followed by incubation at 37 °C for 24 h. On day 2 of transfection, cells were split

into a T25 flask and selected for successful transfection with 2 μg/μL of puromycin (Thermofisher Scientific; A113803) the next day. After 24 h, AMEM media with 10% FBS was changed to the flask to maintain cell proliferation. Cells were subjected to a second time of puromycin selection 7 days later.

2.6. Real-time imaging of insulin signaling using fluorescent microscopy

L6 cells transfected with FoxO1 biosensor were seeded onto a 96-well plate for treatment. When cells reached 50—60% confluency, they were subjected to 6 groups of treatment including control, insulin, iron, iron insulin, salubrinal iron, salubrinal iron insulin. For the iron treatment wells, cells were treated with $FeSO_4$ 250 μM overnight. For the salubrinal iron treatment groups, cells were subjected to salubrinal 30 μM for 30 min prior to overnight iron treatment. After incubation time, cells in all treatment groups were starved in 0% FBS AMEM for 90 min, then treated with 100 nM insulin and imaged on EVOS FL Auto 2 for green fluorescence over a span of 30 min to observe fluorescent translocation. Nuclear fluorescence signal was traced from the nucleus to the cytosol in all treatments with number of cells being 10 for each treatment. Data quantitation was performed using Celleste software.

2.7. Insulin sensitivity measured by glucose uptake assay

Glucose uptake assay was carried out based on the detection of 2-deoxyglucose-6-phosphate (2DG6P). L6-GLUT4myc cells (a kind gift from Dr Amira Klip) were seeded on 96-well plate at 10,000 cells/well before treatment. Cells were then treated with different conditions including: with and without insulin 100 nM, iron, iron insulin, salubrinal, salubrinal insulin, salubrinal iron and salubrinal iron insulin. After 24 h treatment, insulin (100 nM) was stimulated for 15 min 2DG (2-deoxyglucose) was added and incubated for 30 min, followed by addition of stop buffer and neutralization buffer according to the protocol from the Glucose Uptake-Glo Assay kit by Promega. Finally, 2DG6P detection reagent was added and luminescence was recorded.

2.8. ThT staining assay

L6 skeletal muscle cells were seeded at 70% confluency on a μ-slide 4-well chambered polymer coverslip (Ibidi), and the growth medium was then replaced with 0% FBS AMEM (Phenol-red free) and iron treatment (250 μM) for 4 h. After treatment, Tht solution (Sigma—Aldrich; T3516, 2.5 μM) was prepared in phenol-red free DMEM media 0% FBS and imaging with HCS NuclearMask™ Blue Stain (Thermofisher; H10325, 1:2000). Imaging was performed at 20× objective (Nikon A1 confocal microscope) in a 5% CO_2 live-cell chamber.

2.9. GRP-78 mCherry reporter

Cells stably expressing a GRP78 promoter driver mCherry reporter, which we generated previously [31], were seeded on 4-well chamber and subjected to iron treatment (250 μM) for 24 h. Imaging was performed at 20× objective (Nikon A1 confocal microscope) and 1 h intervals up to 24 h in a 5% CO_2 live-cell chamber.

2.10. Gene expression analysis

Total RNA was extracted with RNEasy Mini Kit (Qiagen, Toronto, Canada) and then converted to cDNA using the RevertAid RT Kit (Thermo Scientific; K1691). qPCR was performed with Sso Advanced SYBR Green Master Mix (Bio-Rad; 1725270) starting with an initial activation at 95 °C for 15 min, followed by 40 cycles of 94 °C for 15 s, 55 °C for 30 s and 70 °C for 30 s on a Bio-Rad CFX384 Touch Real-Time PCR Detection System. Relative gene expression levels were normalized to 18S rRNA. Primers used in this study are summarized in Table 1.

Table 1 — List of Primers used.

Name	Kind	Sequences (5′-3′)
ATG5	Forward	CCTGAAGACGGAGAGAAGAAGAG
	Reverse	CGGGAAGCAAGGGTGTCAT
ATG10	Forward	CCTGTTTGCTTGGGATAGTGG
	Reverse	ACTTCCCCATCAATCTCCAC
ATG12	Forward	CATTCTTACCTGGCGTTGAG
	Reverse	CACTTCAAACCCTGTAATCC
ATG16	Forward	CACATCTTTACCCAGCATCAC
	Reverse	CAGGACAGAGGGTGCTTTC
LC3	Forward	TGTTAGGCTTGCTCTTTTGG
	Reverse	GCAGAGGAAATGACCACAGAT
ATF4	Forward	GATGCCTTTTCCGGGACAGA
	Reverse	GGCAGCCTGGTCGACTTTTA
ATG7	Forward	CGAAGGTCAGGAGCAGAAC
	Reverse	AGGCACCCAAAGACATCAAG

2.11. Mouse model of iron overload-induced insulin resistance, glucose tolerance tests (GTT)

Animals were fed ad libitum on regular chow diet and kept in temperature and humidity control rooms with a daily 12:12-h light—dark cycle. 20 8-weeks-old C57/BL6J male mice were categorized into four groups including control, iron, salubrinal and salubrinal iron. Iron dextran (Sigma Aldrich; D8517) was delivered intravenously at 15 mg/kg for three times at 2 h-interval in iron group mice while PBS was used as control. Intraperitoneal injection was performed in salubrinal groups (1 mg/kg) on day 1, day 2 and day 3. For salubrinal iron groups, salubrinal was also injected at 1 mg/kg on day 1, day 2 and day 3. On day 3, iron dextran was delivered intravenously at 15 mg/kg after 30 min of salubrinal injection. For phosphorylation of insulin signaling analysis, all mice were injected via tail vein with insulin (4 units per kg) 5 min before sacrifice. Skeletal muscles were collected and lysed in tissue lysis buffer. For glucose tolerance test, after 24 h of the last iron injections, all mice were injected with glucose at 1 g/kg, followed by blood glucose measurement at different intervals in 2 h 2 primary antibodies were used to detect iron levels in skeletal muscles include Anti-ferritin heavy chain (Novus Biologicals; NBP1-31944) and Anti-transferrin receptor (Tfr1) monoclonal antibody (ThermoFisher; 13-6800).

2.12. Statistical analysis

One-way and two-way ANOVA test with turkey's multiple comparisons was carried out on GraphPad Prism to determine statistical significance in which p values < 0.05 were considered significant.

3. RESULTS

3.1. Iron elevates ER stress and UPR induction in L6 skeletal muscle cells

To investigate the effects of iron on ER stress, we first employed the Tht assay to detect protein aggregates, an established marker of ER stress [24]. In this experiment, L6 skeletal muscle cells were treated with or without 250 μM $FeSO_4$ for 4 h, and Thioflavin T used as a probe to monitor misfolded protein accumulation. Our results show fluorescence was significantly enhanced, indicative of protein aggregates, in iron-treated L6 skeletal muscle cells (Figure 1A&B). Next, we examined the effects of iron overload on the unfolded protein response (UPR). To

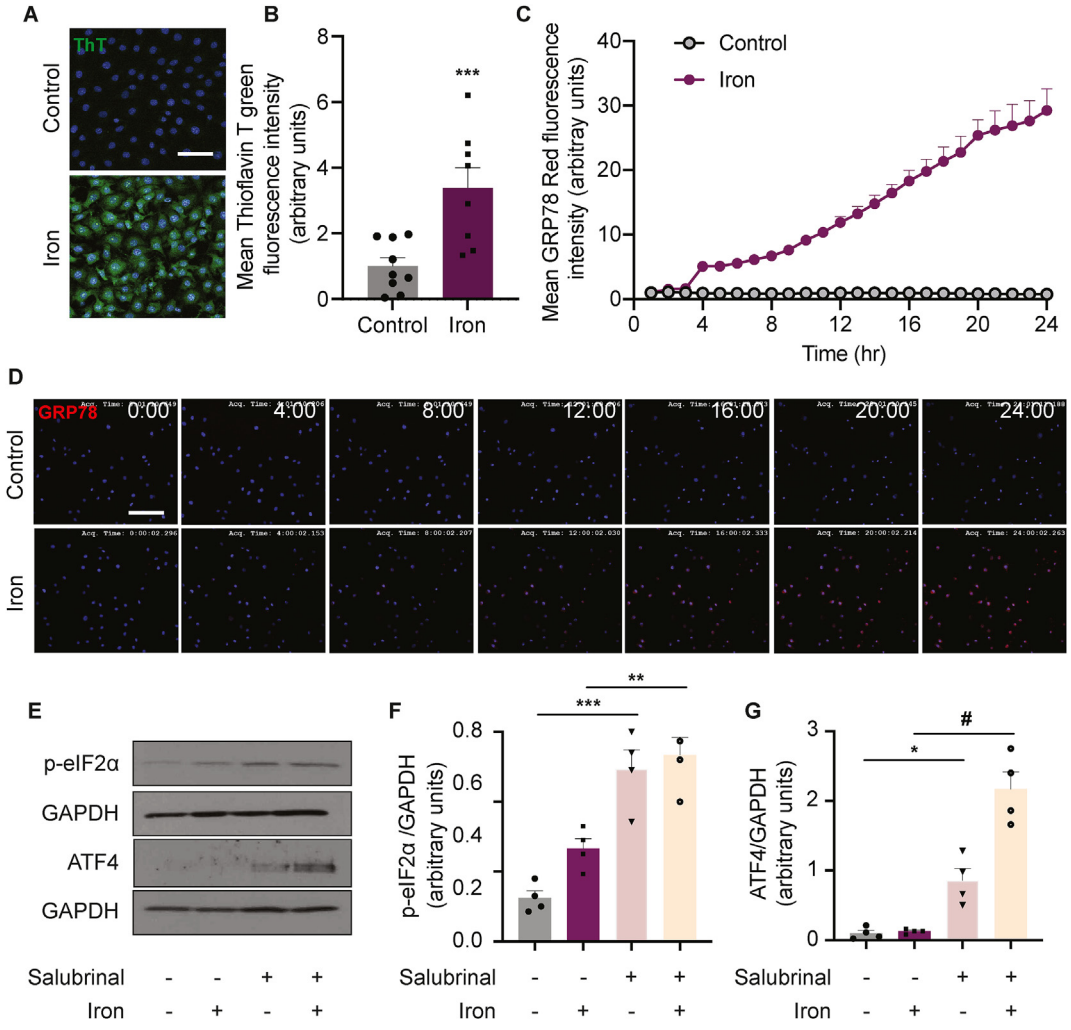

Figure 1: Effect of iron overload and salubrinal on ER stress and UPR activation.
A-B. Representative confocal images and quantification of Tht assay measuring protein aggregates in L6 skeletal muscle cells after iron injections ($FeSO_4$, 250 μM, 4 h) compared to control. C-D. Representative confocal images and quantification of L6 GRP78- mCherry reporter and quantification of mean red fluorescence for 24 h iron treatment compared to control. Scale bar (confocal microscope) = 10 μm. E. Representative Western blot images of phospho-eIF2α and ATF4 over GAPDH after iron treatment (250 μM, 24 h), with and without salubrinal treatment (30 μM, 30 min). F. Quantification of phospho-eIF2α over GAPDH after iron treatment (250 μM, 24 h), with and without salubrinal treatment (30 μM, 30 min). Values are mean ± s.e.m (n = 4) **P < 0.005 ***P < 0.0005 (one-way ANOVA with multiple comparisons). G. Quantification of ATF4 over GAPDH with after iron treatment (250 μM, 24 h), with and without salubrinal pretreatment (30 μM, 30 min). Values are mean ± s.e.m (n = 4) *P < 0.05 #P < 0.0001 (one-way ANOVA with multiple comparisons).

do so we generated L6 skeletal muscle cells stably expressing a GRP78 promoter-driven mCherry reporter. Time lapse imaging indicated a rapid increase in response to iron compared with control cells, which was apparent after 4 h and maintained up to 24 h treatment (Figure 1C&D). To verify the effectiveness of salubrinal we then used Western blotting (Figure 1E–G) to demonstrate that it induces a significant increase in phosphorylation of p-eIF2α and ATF4 level. This confirms salubrinal caused an increase in UPR activation, specifically via the eIF2α-ATF4 pathway. There was no significant effect of iron alone on p-eIF2α and ATF4 level, although an apparent small increase of p-eIF2α was observed (Figure 1E–G).

3.2. Iron impairs insulin sensitivity in L6 skeletal muscle cells; an effect prevented upon salubrinal treatment

We analyzed kinetics of insulin sensitivity by generating L6 cell clones overexpressing an Akt biosensor combined with real-time analysis of fluorescence. This biosensor is based upon measure of phosphorylated FoxO1 translocation from the nucleus to cytosol. Our representative images (Figure 2A) visually reflected the difference in nuclear fluorescence intensity over a time-span of 20 min. Quantification indicated that insulin-stimulated Akt activity was significantly reduced in cells treated with insulin compared to control cells (Figure 2B&C). Both temporal analysis (Figure 2B) and quantitation after 20 min (Figure 2C) showed that iron caused insulin-resistance and that salubrinal pretreatment attenuated this effect of iron. Insulin sensitivity was also assessed by Western blot analysis and our results show that there was a significant decrease in insulin-stimulated phosphorylation of Akt s473 (Figure 2D) as well as ERK (Figure 2E) upon iron treatment. Upon salubrinal pretreatment, improved insulin stimulated Akt s473 and ERK was observed, confirming the ability of salubrinal in rescuing insulin sensitivity upon iron overload. Insulin resistance in skeletal muscle is manifested by decreased insulin-stimulated glucose uptake and to test

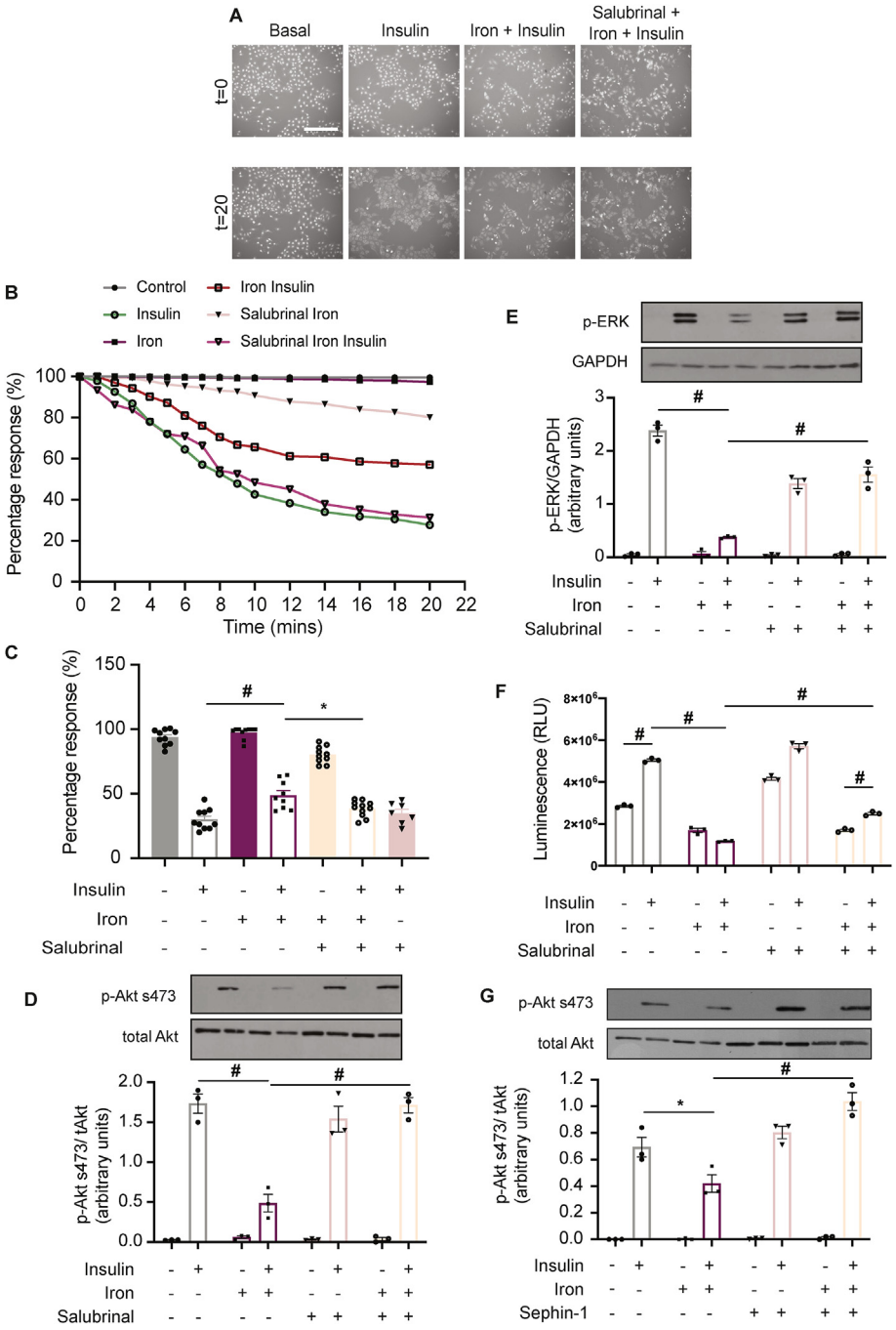

Figure 2: Effect of iron and salubrinal on insulin sensitivity.
A. Representative microscope images of biosensor cells recorded at timepoints t = 0 and t = 20 (min) with insulin stimulation (100 nM, 10 min) after iron treatment (250 μM, 24 h) with and without salubrinal pretreatment (30 μM, 30 min) All experiments were repeated three times. Scale bar = 100 μm. B. Percentage change of green nuclear fluorescent signal in biosensor cells (n = 10) recorded for a timecourse of 20 min with insulin stimulation (100 nM, 10 min) after iron treatment (250 μM, 24 h) with and without salubrinal pretreatment (30 μM, 30 min). Percentage change was recorded as mean values. C. Percentage response (%) of green fluorescent signal in biosensor cells (n = 10) recorded for a timecourse of 20 min with insulin stimulation (100 nM) after iron treatment (250 μM, 24 h) with and without salubrinal pretreatment (30 μM, 30 min). Values are mean ± s.e.m *P < 0.05 #P < 0.0001 (one-way ANOVA with multiple comparisons). D. Representative Western blot images and quantification of phospho-Akt (s473) over total Akt with insulin stimulation (100 nM, 10 min) after iron treatment (250 μM, 24 h) with and without salubrinal pretreatment (30 μM, 30 min). Values are mean ± s.e.m (n = 3) #P < 0.001 (two-way ANOVA with multiple comparisons). E. Representative Western blot images and quantification of phospho-ERK over GAPDH with insulin stimulation (100 nM, 10 min) after iron treatment (250 μM, 24 h) with and without salubrinal pretreatment (30 μM, 30 min). Values are mean ± s.e.m (n = 3) #P < 0.001 (two-way ANOVA with multiple comparisons). F. Glucose uptake of L6 skeletal muscle cells with insulin stimulation (100 nM, 20 min) after iron treatment (250 μM, 24 h) with and without salubrinal pretreatment (30 μM, 30 min). Values are mean ± s.e.m. #P < 0.0001 (two-way ANOVA with multiple comparisons). G. Representative Western blot images and quantification of phospho-Akt (s473) over total Akt with insulin stimulation (100 nM, 10 min) after iron treatment (250 μM, 24 h) with and without sephin1 pretreatment (10 μM, 30 min). Values are mean ± s.e.m (n = 3) *P < 0.05 #P < 0.0001 (two-way ANOVA with multiple comparisons).

the functional significance of our previous observations we next examined glucose uptake. A significant reduction in insulin-stimulated glucose uptake was found upon iron pretreatment for 24 h (Figure 2F). Salubrinal pretreatment elicited a significantly elevated insulin response in the presence of iron. To avoid potential contribution of off-target inhibitory effects we used sephin1, another distinct eIF2α phosphatase inhibitor, to further validate the importance of eIF2α phosphorylation in improving insulin sensitivity upon iron overload (Figure 2G). Together, these results demonstrate the detrimental consequence of iron overload on skeletal muscle cell insulin sensitivity and the beneficial effect of salubrinal in attenuating insulin resistance.

3.3. Autophagy initiation and flux is upregulated in L6 skeletal muscle cells upon salubrinal treatment

We first used qPCR to examine changes in level of autophagy-related gene 5 (ATG5), autophagy-related gene 10 (ATG10), autophagy-related gene 12 (ATG12), autophagy-related gene 16 (ATG16) and unc-51 like autophagy activating kinase 1 (ULK1). Heat map of scaled data (Figure 3A) shows that salubrinal alone most strongly increased the expression of ATG5, ATG12 and ATG10 compared to basal, while iron plus salubrinal had highest effect on ATG16 and ULK1 mRNA expression level. The effect of iron and salubrinal on autophagic flux was also investigated by measuring LC3 and p62 by Western blot (Figure 3B&C). Data shows that both iron and salubrinal significantly increased formation of autophagosomes, as indicated by increased LC3-II detection (Figure 3B). However, we observed a significant increase in p62 only upon iron treatment, indicating a block of autophagic flux (Figure 3C). This iron-induced accumulation of p62 was significantly downregulated upon pretreatment with salubrinal. To further investigate autophagic flux, L6 cells stably expressing LC3B-eGFP-mCherry were assessed. In this assay, eGFP signal was quenched by the acidic environment upon autophagosome and lysosome fusion, while mCherry fluorescence remains stable. Incorporating this cell line with our cellular treatment model, a significant increase in number of eGFP and mCherry fluorescence puncta after 24 h iron treatment was observed, validating inhibition of flux. Salubrinal pretreatment, however, resulted in a significant elevation of mCherry fluorescence accompanied by a reduction of fluorescence puncta upon iron overload (Figure 3D—F). This observation confirmed the potency of salubrinal in inducing autophagic flux.

To test whether autophagy is critical for the beneficial effect of salubrinal in alleviating insulin sensitivity, we used a loss of function approach by generating two cellular models. Both overexpression of a dominant-negative ATG5K130R mutant and knockout of ATG7 were used to generate autophagy-deficiency. Analysis of insulin sensitivity by Western blotting demonstrated that iron-impaired insulin sensitivity could be attenuated by salubrinal in cells transfected with empty vector but not in autophagy-deficient ATG5K130R overexpressing cells (Figure 3 G&H). Similarly, knockout of ATG7 effectively blocked the capacity of salubrinal to rescue insulin sensitivity (Figure 3 I&J). To further validate the significance of autophagy in enhancing insulin sensitivty, we used a gain of function approach with Tat beclin-1 as an activator of autophagy, with and without iron treatment. Accordingly, a reduction in iron-induced insulin resistance was observed when autophagy was induced by Tat beclin-1 (Figure 3K). Taken together, our results suggest that induction of autophagy flux by salubrinal is essential to alleviate IO-induced ER stress and insulin resistance in L6 skeletal muscle cells.

3.4. Salubrinal promotes UPR activation and autophagy flux thus alleviating IO-induced insulin resistance in mice

Mice with or without intraperitoneal salubrinal pretreatment and with or without systemic iron administration were injected with insulin (4 units per kg), 5 min before sacrifice as depicted in Figure 4A. As expected, a significant elevation in skeletal muscle ferritin levels was observed while TfR1 expression was significantly downregulated in IO mice (Figure 4B—D). Glucose tolerance test was used to show that IO impaired insulin sensitivity in mice. The use of salubrinal preserved insulin sensitivity following IO (Figure 4E&F). Moreover, Western blotting showed that iron reduced insulin-stimulated phosphorylation of Akt s473 and ERK, while salubrinal pretreatment attenuated this development of insulin resistance, recapitulating the results of studies in L6 skeletal muscle cells reported above (Figure 4G—I). Results also showed that there was an increase in both phosphorylation of eIF2α and ATF4 levels (Figure 4J-L) in the salubrinal and iron-injected mice, indicative of UPR activation upon salubrinal and iron administration. We further analyzed autophagic flux by Western blotting of LC3B and p62 expression. In iron-injected mice, an apparent increase in both LC3B-II and p62 expression was observed, indicating impaired autophagy flux, compared to control mice. However, with salubrinal administration, expression of LC3B-II and p62 were significantly downregulated, suggesting enhancement of autophagy flux, both in the presence and absence of iron (Figure 4N-P). Our result was also corroborated with qPCR heatmap depicting a significant upregulation in the UPR and autophagy-related genes (Figure 4M). Collectively, these data indicate that salubrinal injection in mice resembled key observations of our L6 cell culture model.

4. DISCUSSION

Iron homeostasis imbalance is still a somewhat underappreciated contributor to various diseases, including cancer, inflammation, neurodegenerative diseases, and most notably cardiometabolic dysfunction [32]. Indeed, a dysmetabolic iron overload syndrome (DIOS) has been defined since elevated iron levels are observed in 15% of metabolic syndrome patients and in half of those with non-alcoholic fatty liver disease (NAFLD) [33,34]. Nevertheless, the precise mechanisms linking iron overload with such adverse metabolic outcomes remain to be fully understood. In this study we present new knowledge that salubrinal can attenuate iron-induced insulin resistance in skeletal muscle cells. Translating this to an animal model of iron overload, we observed that insulin responsiveness was improved by salubrinal.

Of particular relevance for this study is the impact of iron overload on skeletal muscle. Iron overload can lead to skeletal muscle atrophy, sarcopenia, reduced power and performance, and has been implicated in muscular dystrophy [35—38]. It has been proposed that in addition to direct metabolic effects, iron overload in skeletal muscle may also impact its endocrine function [39]. Collectively, this means that excess iron on skeletal muscle can impact a wide array of pathophysiological outcomes. We have shown that iron overload induced insulin resistance both in mice and cultured skeletal muscle cells [15]. This involved a decrease in Akt-mediated repression of TSC2, resulting in a potent repression of RHEB and mTORC1, with consequent loss of autophagosome lysosome reformation (ALR). This identified mTOR-UVRAG-dependent lysosomal pool regeneration as a determinant of skeletal muscle insulin sensitivity, and demonstrated an important role for autophagic flux in improving insulin sensitivity. Other studies have

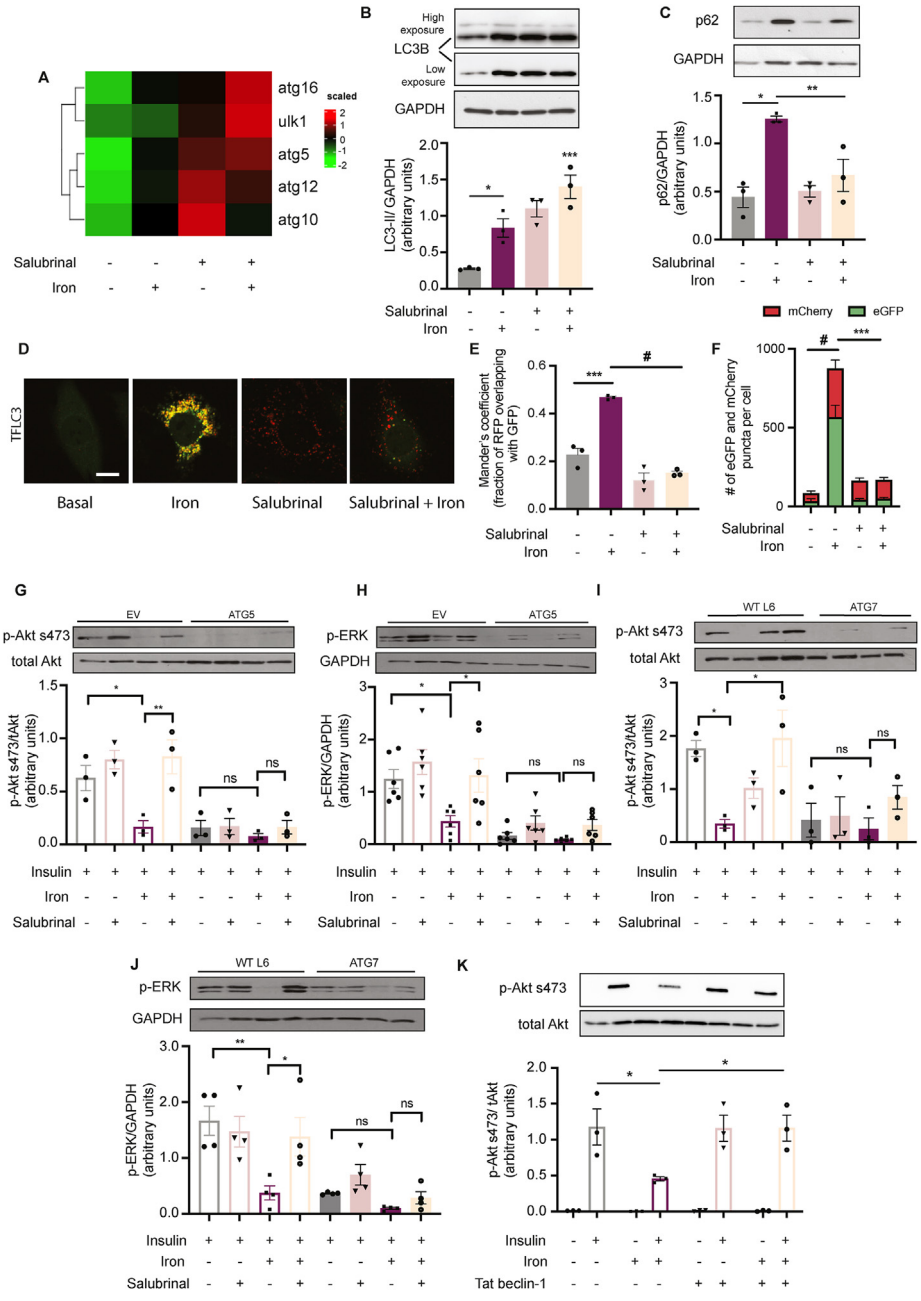

Figure 3: Effect of iron and salubrinal on autophagy.

A. Relative gene expressions— autophagy-related gene 5 (ATG5), autophagy-related gene 10 (ATG10), autophagy-related gene 12 (ATG12), autophagy-related gene 16 (ATG16) and unc-51 like autophagy activating kinase 1 (ULK1)- normalized to 18S rRNA expression with iron treatment (250 μM, 24 h), with and without salubrinal pretreatment (30 μM, 30 min). B. Representative Western blot images and quantification of LC3B-II over GAPDH in L6 skeletal muscle cells after iron treatment (250 μM, 16 h), with and without salubrinal pre-treatment (30 μM, 30 min). Values are mean ± s.e.m (n = 3) *P < 0.05 ***P < 0.0005 (one-way ANOVA with multiple comparisons). C. Representative Western blot images and quantification of p62 over GAPDH in L6 skeletal muscle cells after iron treatment (250 μM, 16 h), with and without salubrinal pre-treatment (30 μM, 30 min). Values are mean ± s.e.m (n = 3) *P < 0.05 **P < 0.005 (one-way ANOVA with multiple comparisons). D. Representative confocal images of L6 cells stably expressing tandem fluorescent-eGFP-mCherry LC3 after iron treatment (250 μM, 24 h) with and without salubrinal pretreatment (30 μM, 30 min). Scale bar denotes 20 μm. E. Mander's coefficient (fraction of RFP channel overlapping GFP). Values are mean ± s.e.m (n = 3) ***P < 0.0005 #P < 0.0001 (one-way ANOVA with multiple comparisons). F. Quantification of eGFP-mCherry LC3 puncta. Values are mean ± s.e.m (n = 3) ***P < 0.0005 #P < 0.0001 (one-way ANOVA with multiple comparisons). G. Representative Western blot images and quantification of phospho-Akt (S473) over total Akt in EV and ATG5 cells with insulin stimulation (100 nM, 10 min) after iron treatment (250 μM, 24 h) with and without salubrinal pretreatment (30 μM, 30 min). Values are mean ± s.e.m (n = 3) *P < 0.05 **P < 0.005 (one-way ANOVA with multiple comparisons). H. Representative Western blot images and quantification of phospho-ERK over GAPDH in EV and ATG5 cells with insulin stimulation (100 nM, 10 min) after iron treatment (250 μM, 24 h) with and without salubrinal pretreatment (30 μM, 30 min). Values are mean ± s.e.m (n = 5) *P < 0.05 **P < 0.005 (one-way ANOVA with multiple comparisons). I. Representative Western blot images and quantification of phospho-Akt (S473) over total Akt in L6 and ATG7 cells with insulin stimulation (100 nM, 10 min) after iron treatment (250 μM, 24 h) with and without salubrinal pretreatment (30 μM, 30 min). Values are mean ± s.e.m (n = 3) *P < 0.05 (one-way ANOVA with multiple comparisons). J. Representative Western blot images and quantification of phospho-ERK over GAPDH in L6 and ATG7 cells with insulin stimulation (100 nM, 10 min) after iron treatment (250 μM, 24 h) with and without salubrinal pretreatment (30 μM, 30 min). Values are mean ± s.e.m (n = 4) *P < 0.05 **P < 0.005 (one-way ANOVA with multiple comparisons). K. Representative Western blot images and quantification of phospho-Akt (s473) over total Akt with insulin stimulation (100 nM, 10 min) after iron treatment (250 μM, 24 h) with and without tat-beclin 1 pretreatment (5 μM, 24 h). Values are mean ± s.e.m (n = 3) *P < 0.05 (two-way ANOVA with multiple comparisons).

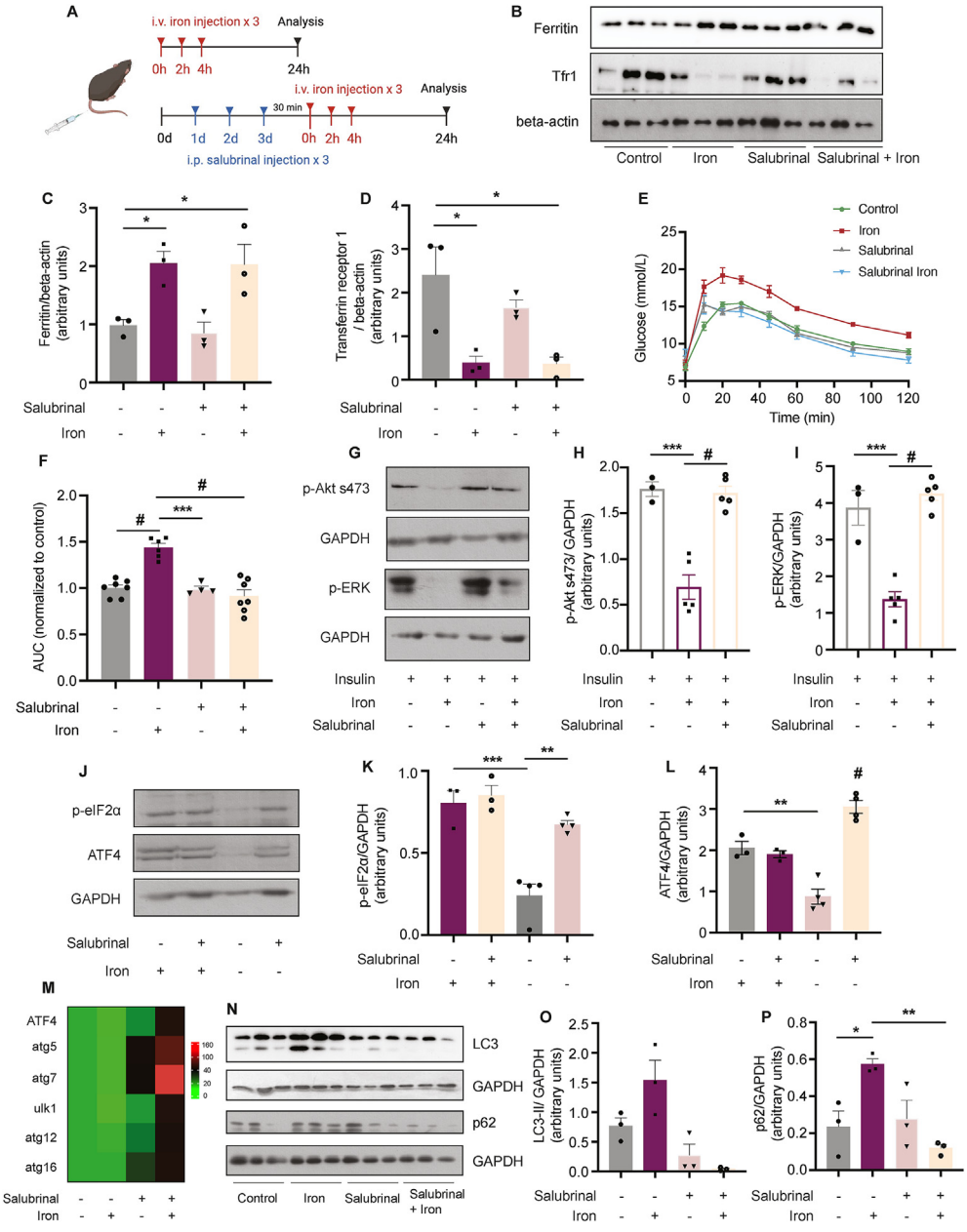

Figure 4: In vivo model of mice skeletal muscles with IO.

A. Schematic diagram of salubrinal-iron injections' experimental plan. B. Representative Western blot images of ferritin and Tfr1 over beta-actin in skeletal muscles after iron injection, with and without salubrinal administration. C. Quantification of Ferritin over beta-actin in L6 skeletal muscles after iron injection, with and without salubrinal administration. Values are mean ± s.e.m (n = 3) *P < 0.05 (one-way ANOVA with multiple comparisons). D. Quantification of Tfr1 over beta-actin in L6 skeletal muscles after iron injection, with and without salubrinal administration. Values are mean ± s.e.m (n = 3) *P < 0.05 (one-way ANOVA with multiple comparisons). E. Glucose tolerance test (GTT) 24-h after iron injections. F. Quantification of area under curve for GTT ***P < 0.0005 #P < 0.0001 (one-way ANOVA with multiple comparisons). G. Representative Western blot images of phospho-Akt (S473) and phospho-ERK over GAPDH in skeletal muscles after iron injection followed by i.p. insulin injection with and without salubrinal injection. H. Quantification of phospho-Akt (S473) over GAPDH in skeletal muscles after iron injection followed by i.p. insulin injection with and without salubrinal injection. Values are mean ± s.e.m (n = 5) ***P < 0.0005 #P < 0.0001 (one-way ANOVA with multiple comparisons). I. Quantification of phospho-ERK over GAPDH in skeletal muscles after iron injection followed by i.p. insulin injection with and without salubrinal injection. Values are mean ± s.e.m (n = 5) ***P < 0.0005 #P < 0.0001 (one-way ANOVA with multiple comparisons). J. Representative Western blot images of phospho-eIF2α and ATF4 over GAPDH in skeletal muscles after iron injection followed by i.p. insulin injection with and without salubrinal injection. K. Quantification of phospho-eIF2α over GAPDH in skeletal muscles after iron injection followed by i.p. insulin injection with and without salubrinal injection. Values are mean ± s.e.m (n = 3) **P < 0.005 ***P < 0.0005 (one-way ANOVA with multiple comparisons). L. Quantification of ATF4 over GAPDH in skeletal muscles after iron injection followed by i.p. insulin injection with and without salubrinal injection. Values are mean ± s.e.m (n = 3) **P < 0.005 #P < 0.0001 (one-way ANOVA with multiple comparisons). M. Relative gene expressions— activating transcription factor 4 (ATF4), autophagy-related gene 5 (ATG5), autophagy-related gene 7 (ATG7), autophagy-related gene 12 (ATG12), autophagy-related gene 16 (ATG16) and unc-51 like autophagy activating kinase 1 (ULK1)- normalized to 18S rRNA expression. N. Representative Western blot images of LC3B and p62 over GAPDH in skeletal muscles after iron injection, with and without salubrinal administration. O. Quantification of LC3B-II over GAPDH in L6 skeletal muscles after iron injection, with and without salubrinal administration. Values are mean ± s.e.m (n = 3). P. Quantification of p62 over GAPDH in L6 skeletal muscles after iron injection, with and without salubrinal administration. Values are mean ± s.e.m (n = 3) *P < 0.05 **P < 0.005 (one-way ANOVA with multiple comparisons). O. Relative gene expressions— activating transcription factor 4 (ATF4), autophagy-related gene 5 (ATG5), autophagy-related gene 7 (ATG7), autophagy-related gene 12 (ATG12), autophagy-related gene 16 (ATG16) and unc-51 like autophagy activating kinase 1 (ULK1)- normalized to 18S rRNA expression.

documented the association of autophagy and insulin sensitivity, with strategies to promote autophagy flux conferring improved responsiveness [31,40–45]. Thus, inhibition of autophagy is an important means via which iron attenuates insulin sensitivity.

Several previous studies using models from yeast to mammalian cells and tissues have shown, as we did here, that iron could cause endoplasmic reticulum stress [46,47]. For example, in mouse hippocampal neuronal cells iron induced ER stress leading to mitochondrial fragmentation and neuronal cell death [48]. Lipocalin-2 mediated iron accumulation in pulmonary arterial smooth muscle cells and hypoxia-induced iron accumulation in oligodendrocytes both led to ER stress [49,50]. Induction of ER stress led to insulin resistance in L6 and C2C12 skeletal muscle cells [51,52], murine preadipocytes [53], hepatocytes [54], and was associated with reduced insulin sensitivity in db/db mice [55]. Upregulation of tribbles 3 (TRB3) and inhibition of the skeletal muscle-enriched inositol polyphosphate phosphatase (SKIP) with suppression of insulin receptors' transportation to the cell surface are potential mechanistic pathway linking ER stress and insulin resistance [56–58]. Strategies to counteract cellular ER stress, either endogenous homeostatic mechanisms or therapeutic interventions, are clearly of widespread potential benefit.

To alleviate ER stress and restore optimal homeostasis, an endogenous cellular response is activation of the UPR which can lead to corrective mechanisms including suppressing protein translation, inducing the production of molecular chaperones involved in protein folding and degrading misfolded proteins via routes such as induction of autophagy. A study in 3T3-L1 adipocytes suggested that induction of autophagy by UPR was important for maintenance of insulin sensitivity [44]. One of the three main branches of the UPR involves the eukaryotic translation initiation factor 2 alpha (eIF2α) [59,60]. In this study we found that iron induced UPR activation, as observed by an increase in the expression of the GRP78 promoter-dependent fluorescent reporter. Our results were corroborated with Western blot analysis showing an increase in phosphorylation of eIF2α and increased ATF4. However, although UPR was induced in response to iron, we found that the normal increase in autophagy flux in response to UPR activation was prevented by iron. Thus, via ALR attenuation, iron effectively suppressed a critical endogenous corrective cellular response which is designed to restore insulin sensitivity.

Exercise has been proposed as a potential means of promoting autophagy to alleviate ER stress and increase insulin sensitivity [61]. Effects of exercise are variable, and we contend a more direct and controlled route would be advantageous. eIF2α can be activated using salubrinal, a small molecule protein phosphatase 1C inhibitor which maintains eIF2α phosphorylation. Via enhancing PERK/eIF2α/ATF4 signaling, salubrinal has been suggested as a potential therapeutic approach for hypoxia-induced retinal microangiopathy, neuroprotection and in cerebral ischemia [62–66]. In our study we found in

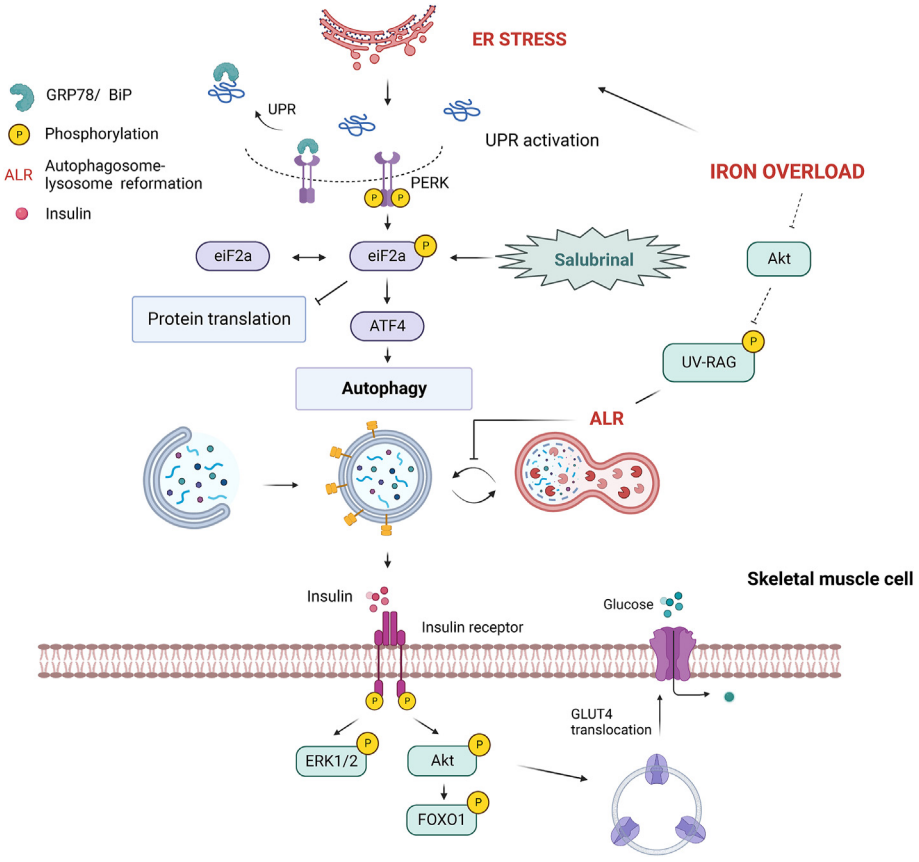

Figure 5: Schematic diagram of ER-stress induced iron overload leading to insulin resistance.
Iron-overload causes ER stress in L6 skeletal muscle cells and the subsequent UPR activation. Iron-overload also causes impaired autophagic flux through impaired autophagosome lysosome reformation (ALR), leading to insulin resistance. Salubrinal, an eIF2α phosphatase inhibitor, induces UPR activation, specifically the eIF2α and ATF4 pathway, resulting in improved autophagic flux and insulin sensitivity, both in the presence and absence of iron.

the L6 cell model that salubrinal stimulated eIF2α-mediated induction of autophagy and that this attenuated the extent of insulin resistance caused by iron. Furthermore, administration of salubrinal to mice before systemic injection of iron could attenuate development of insulin resistance in skeletal muscle. These data validate, using a pharmacological approach, the potential of therapeutically targeting eIF2α to promote improved insulin responsiveness. Ideally, precise analysis of insulin sensitivity using hyperinsulinemic-euglycemic clamp would provide more sensitive and robust support for this conclusion.

In summary, we have established that skeletal muscle cells treated with iron or skeletal muscle of mice with iron overload develop ER stress and insulin resistance. By virtue of also suppressing autophagy, iron prevents the ability of endogenous UPR to enhance autophagic flux and restore cellular homeostasis (Figure 5). We found that directly promoting eIF2α-dependent activation of UPR and autophagy with salubrinal prior to iron exposure could attenuate development of insulin resistance. New knowledge from this study identifies the potential use of salubrinal to improve insulin sensitivity in metabolic syndrome patients with iron overload.

CREDIT AUTHORSHIP CONTRIBUTION STATEMENT

Khang Nguyen: Writing — original draft, Visualization, Investigation, Formal analysis, Data curation. **Jialing Tang:** Methodology, Investigation, Formal analysis, Data curation. **Sungji Cho:** Methodology, Investigation, Formal analysis, Data curation. **Fan Ying:** Investigation, Formal analysis. **Hye Kyoung Sung:** Supervision, Project administration, Investigation. **James Wonsuk Jahng:** Investigation, Formal analysis, Data curation. **Kostas Pantopoulos:** Writing — review & editing, Methodology, Conceptualization. **Gary Sweeney:** Writing — review & editing, Supervision, Resources, Project administration, Methodology, Funding acquisition, Conceptualization.

ACKNOWLEDGEMENTS

GS thanks Canadian Institutes of Health Research, International Development Research Council and National Science and Engineering Research Council for research funding.

DECLARATION OF COMPETING INTEREST

The authors declare that they have no known competing financial interests or personal relationships that could have appeared to influence the work reported in this paper.

DATA AVAILABILITY

Data will be made available on request.

REFERENCES

[1] Abbaspour N, Hurrell R, Kelishadi R. Review on iron and its importance for human health. J Res Med Sci: Off J Isfahan Univ Med Sci 2014;19(2):164.
[2] Wallace DF. The regulation of iron absorption and homeostasis. Clin Biochem Rev 2016;37(2):51.
[3] Taher AT, Saliba AN. Iron overload in thalassemia: different organs at different rates. Hematology 2017;2017(1):265—71. the American Society of Hematology Education Program Book.
[4] Gattermann N. Iron overload in myelodysplastic syndromes (MDS). Int J Hematol 2018;107(1):55—63.
[5] Zeltmacher K, Bevans M. Aplastic anemia and its association with hemochromatosis. Arch Intern Med 1945;75(6):395—403.
[6] Vela D. Iron metabolism in prostate cancer; from basic science to new therapeutic strategies. Front Oncol 2018;547.
[7] Cornelissen A, Guo L, Sakamoto A, Virmani R, Finn AV. New insights into the role of iron in inflammation and atherosclerosis. EBioMedicine 2019;47:598—606.
[8] Sipe JC, Lee P, Beutler E. Brain iron metabolism and neurodegenerative disorders. Dev Neurosci 2002;24(2—3):188—96.
[9] Padwal MK, Murshid M, Nirmale P, Melinkeri RR. Association of serum ferritin levels with metabolic syndrome and insulin resistance. J Clin Diagn Res: J Clin Diagn Res 2015;9(9):BC11.
[10] Simcox JA, McClain DA. Iron and diabetes risk. Cell Metabol 2013;17(3):329—41.
[11] Ormazabal V, Nair S, Elfeky O, Aguayo C, Salomon C, Zuñiga FA. Association between insulin resistance and the development of cardiovascular disease. Cardiovasc Diabetol 2018;17(1):1—14.
[12] Kahn BB, Flier JS. Obesity and insulin resistance. J Clin Invest 2000;106(4):473—81.
[13] Båvenholm PN, Kuhl J, Pigon J, Saha AK, Ruderman NB, Efendic S. Insulin resistance in type 2 diabetes: association with truncal obesity, impaired fitness, and atypical malonyl coenzyme A regulation. J Clin Endocrinol Metabol 2003;88(1):82—7.
[14] Riehle C, Abel ED. Insulin signaling and heart failure. Circ Res 2016;118(7):1151—69.
[15] Jahng JWS, Alsaadi RM, Palanivel R, Song E, Hipolito VEB, Sung HK, et al. Iron overload inhibits late stage autophagic flux leading to insulin resistance. EMBO Rep 2019;20(10):e47911.
[16] Sung HK, Song E, Jahng JWS, Pantopoulos K, Sweeney G. Iron induces insulin resistance in cardiomyocytes via regulation of oxidative stress. Sci Rep 2019;9(1):1—13.
[17] Kim JA, Wei Y, Sowers JR. Role of mitochondrial dysfunction in insulin resistance. Circ Res 2008;102(4):401—14.
[18] Mizushima N. Autophagy: process and function. Gene Dev 2007;21(22):2861—73.
[19] Fritzen AM, Madsen AB, Kleinert M, Treebak JT, Lundsgaard AM, Jensen TE, et al. Regulation of autophagy in human skeletal muscle: effects of exercise, exercise training and insulin stimulation. J Physiol 2016;594(3):745—61.
[20] Schwarz DS, Blower MD. The endoplasmic reticulum: structure, function and response to cellular signaling. Cell Mol Life Sci 2016;73(1):79—94.
[21] Hotamisligil GS. Endoplasmic reticulum stress and the inflammatory basis of metabolic disease. Cell 2010;140(6):900—17.
[22] Preissler S, Rato C, Yan Y, Perera LA, Czako A, Ron D. Calcium depletion challenges endoplasmic reticulum proteostasis by destabilising BiP-substrate complexes. Elife 2020;9:e62601.
[23] Lee SY, Lee MS, Cherla RP, Tesh VL. Shiga toxin 1 induces apoptosis through the endoplasmic reticulum stress response in human monocytic cells. Cell Microbiol 2008;10(3):770—80.
[24] Cao SS, Kaufman RJ. Endoplasmic reticulum stress and oxidative stress in cell fate decision and human disease. Antioxidants Redox Signal 2014;21(3):396—413.
[25] Hetz C. The unfolded protein response: controlling cell fate decisions under ER stress and beyond. Nat Rev Mol Cell Biol 2012;13(2):89—102.
[26] Read A, Schröder M. The unfolded protein response: an overview. Biology 2021;10(5):384.
[27] Vembar SS, Brodsky JL. One step at a time: endoplasmic reticulum-associated degradation. Nat Rev Mol Cell Biol 2008;9(12):944—57.
[28] Liu Z, Lv Y, Zhao N, Guan G, Wang J. Protein kinase R-like ER kinase and its role in endoplasmic reticulum stress-decided cell fate. Cell Death Dis 2015;6(7):e1822. e1822.

[29] Rozpedek W, Pytel D, Mucha B, Leszczynska H, Diehl JA, Majsterek I. The role of the PERK/eIF2α/ATF4/CHOP signaling pathway in tumor progression during endoplasmic reticulum stress. Curr Mol Med 2016;16(6):533–44.
[30] Adams CJ, Kopp MC, Larburu N, Nowak PR, Ali MM. Structure and molecular mechanism of ER stress signaling by the unfolded protein response signal activator IRE1. Front Mol Biosci 2019;6:11.
[31] Ahlstrom P, Rai E, Chakma S, Cho HH, Rengasamy P, Sweeney G. Adiponectin improves insulin sensitivity via activation of autophagic flux. J Mol Endocrinol 2017;59(4):339–50.
[32] Fillebeen C, Lam NH, Chow S, Botta A, Sweeney G, Pantopoulos K. Regulatory connections between iron and glucose metabolism. Int J Mol Sci 2020;21(20):7773.
[33] Sachinidis A, Doumas M, Imprialos K, Stavropoulos K, Katsimardou A, Athyros VG. Dysmetabolic iron overload in metabolic syndrome. Curr Pharmaceut Des 2020;26(10):1019–24.
[34] Rametta R, Fracanzani AL, Fargion S, Dongiovanni P. Dysmetabolic hyperferritinemia and dysmetabolic iron overload syndrome (DIOS): two related conditions or different entities? Curr Pharmaceut Des 2020;26(10):1025–35.
[35] Martin D, Nay K, Robin F, Rebillard A, Orfila L, Martin B, et al. Oxidative and glycolytic skeletal muscles deploy protective mechanisms to avoid atrophy under pathophysiological iron overload. Journal of cachexia, sarcopenia and muscle 2022;13(2):1250–61.
[36] Alves FM, Kysenius K, Caldow MK, Hardee JP, Chung JD, Trieu J, et al. Iron overload and impaired iron handling contribute to the dystrophic pathology in models of Duchenne muscular dystrophy. Journal of Cachexia, Sarcopenia and Muscle 2022.
[37] Zhou D, Zhang Y, Mamtawla G, Wan S, Gao X, Zhang L, et al. Iron overload is related to muscle wasting in patients with cachexia of gastric cancer: using quantitative proteome analysis. Med Oncol 2020;37(12):1–11.
[38] Luszczyk M, Kaczorowska-Hac B, Milosz E, Adamkiewicz-Drozynska E, Ziemann E, Laskowski R, et al. Reduction of skeletal muscle power in adolescent males carrying H63D mutation in the HFE gene. BioMed Res Int 2017;2017.
[39] Halon-Golabek M, Borkowska A, Herman-Antosiewicz A, Antosiewicz J. Iron metabolism of the skeletal muscle and neurodegeneration. Front Neurosci 2019;165.
[40] Cui D, Drake JC, Wilson RJ, Shute RJ, Lewellen B, Zhang M, et al. A novel voluntary weightlifting model in mice promotes muscle adaptation and insulin sensitivity with simultaneous enhancement of autophagy and mTOR pathway. Faseb J 2020;34(6):7330–44.
[41] Li B, Wu X, Chen H, Zhuang C, Zhang Z, Yao S, et al. miR199a-5p inhibits hepatic insulin sensitivity via suppression of ATG14-mediated autophagy. Cell Death Dis 2018;9(3):1–15.
[42] Wang Y, Hu Y, Sun C, Zhuo S, He Z, Wang H, et al. Down-regulation of Risa improves insulin sensitivity by enhancing autophagy. Faseb J 2016;30(9):3133–45.
[43] Shi L, Zhang T, Zhou Y, Zeng X, Ran L, Zhang Q, et al. Dihydromyricetin improves skeletal muscle insulin sensitivity by inducing autophagy via the AMPK-PGC-1α-Sirt3 signaling pathway. Endocrine 2015;50(2):378–89.
[44] Zhang Y, Ye M, Chen LJ, Li M, Tang Z, Wang C. Role of the ubiquitin-proteasome system and autophagy in regulation of insulin sensitivity in serum-starved 3T3-L1 adipocytes. Endocr J 2015. EJ15-0030.
[45] Liu Y, Palanivel R, Rai E, Park M, Scheid MP, Sweeney G. Adiponectin stimulates autophagy and reduces oxidative stress to enhance insulin sensitivity during high-fat diet feeding in mice. Diabetes 2015;64(1):36–48.
[46] Wu L, Ding Q, Wang X, Li P, Fan N, Zhou Y, et al. Visualization of dynamic changes in labile iron (II) pools in endoplasmic reticulum stress-mediated drug-induced liver injury. Anal Chem 2019;92(1):1245–51.
[47] Cohen N, Breker M, Bakunts A, Pesek K, Chas A, Argemí J, et al. Iron affects Ire1 clustering propensity and the amplitude of endoplasmic reticulum stress signaling. J Cell Sci 2017;130(19):3222–33.
[48] Lee DG, Kam MK, Kim KM, Kim HS, Kwon OS, Lee HS, et al. Peroxiredoxin 5 prevents iron overload-induced neuronal death by inhibiting mitochondrial fragmentation and endoplasmic reticulum stress in mouse hippocampal HT-22 cells. Int J Biochem Cell Biol 2018;102:10–9.
[49] Wang G, Liu S, Wang L, Meng L, Cui C, Zhang H, et al. Lipocalin-2 promotes endoplasmic reticulum stress and proliferation by augmenting intracellular iron in human pulmonary arterial smooth muscle cells. Int J Biol Sci 2017;13(2):135.
[50] Rathnasamy G, Murugan M, Ling EA, Kaur C. Hypoxia-induced iron accumulation in oligodendrocytes mediates apoptosis by eliciting endoplasmic reticulum stress. Mol Neurobiol 2016;53(7):4713–27.
[51] Eo H, Valentine RJ. Imoxin inhibits tunicamycin-induced endoplasmic reticulum stress and restores insulin signaling in C2C12 myotubes. Am J Physiol Cell Physiol 2021;321(2):C221–9.
[52] Srinivasan V, Tatu U, Mohan V, Balasubramanyam M. Molecular convergence of hexosamine biosynthetic pathway and ER stress leading to insulin resistance in L6 skeletal muscle cells. Mol Cell Biochem 2009;328(1):217–24.
[53] Park TJ, Park SY, Lee HJ, Abd El-Aty AM, Jeong JH, Jung TW. α-ketoisocaproic acid promotes ER stress through impairment of autophagy, thereby provoking lipid accumulation and insulin resistance in murine preadipocytes. Biochem Biophys Res Commun 2022;603:109–15.
[54] Tong X, Zhang Q, Wang L, Ji Y, Zhang L, Xie L, et al. RNF186 impairs insulin sensitivity by inducing ER stress in mouse primary hepatocytes. Cell Signal 2018;52:155–62.
[55] Zhou T, Cheng Y, Yan W, Shi X, Xu X, Zhou J, et al. TSPA as a novel ATF6α translocation inducer efficiently ameliorates insulin sensitivity restoration and glucose homeostasis in db/db mice. Biochem Biophys Res Commun 2018;499(4):948–53.
[56] Koh HJ, Toyoda T, Didesch MM, Lee MY, Sleeman MW, Kulkarni RN, et al. Tribbles 3 mediates endoplasmic reticulum stress-induced insulin resistance in skeletal muscle. Nat Commun 2013;4(1):1–11.
[57] Ijuin T, Hosooka T, Takenawa T. Phosphatidylinositol 3, 4, 5-trisphosphate phosphatase SKIP links endoplasmic reticulum stress in skeletal muscle to insulin resistance. Mol Cell Biol 2016;36(1):108–18.
[58] Brown M, Dainty S, Strudwick N, Mihai AD, Watson JN, Dendooven R, et al. Endoplasmic reticulum stress causes insulin resistance by inhibiting delivery of newly synthesized insulin receptors to the cell surface. Mol Biol Cell 2020;31(23):2597–629.
[59] Proud CG. eIF2 and the control of cell physiology. Semin Cell Dev Biol 2005;16(1):3–12 [Academic Press].
[60] Komar AA, Merrick WC. A retrospective on EIF2A—and not the alpha subunit of EIF2. Int J Mol Sci 2020;21(6):2054.
[61] Cheng F, Dun Y, Cheng J, Ripley-Gonzalez JW, Jiang W, You B, et al. Exercise activates autophagy and regulates endoplasmic reticulum stress in muscle of high-fat diet mice to alleviate insulin resistance. Biochem Biophys Res Commun 2022;601:45–51.
[62] Zhang J, Wang Y, Ju M, Song J, Zheng Y, Lin S, et al. Neuroprotective effect of the inhibitor salubrinal after cardiac arrest in a rodent model. Oxid Med Cell Longev 2020;2020.
[63] Anuncibay-Soto B, Pérez-Rodriguez D, Santos-Galdiano M, Font-Belmonte E, Ugidos IF, Gonzalez-Rodriguez P, et al. Salubrinal and robenacoxib treatment after global cerebral ischemia. Exploring the interactions between ER stress and inflammation. Biochem Pharmacol 2018;151:26–37.
[64] Hu Y, Lu X, Xu Y, Lu L, Yu S, Cheng Q, et al. Salubrinal attenuated retinal neovascularization by inhibiting CHOP-HIF1α-VEGF pathways. Oncotarget 2017;8(44):77219.
[65] Barreda-Manso MA, Yanguas-Casás N, Nieto-Sampedro M, Romero-Ramírez L. Neuroprotection and blood–brain barrier restoration by salubrinal after a cortical stab injury. J Cell Physiol 2017;232(6):1501–10.
[66] Anuncibay-Soto B, Pérez-Rodríguez D, Santos-Galdiano M, Font E, Regueiro-Purriños M, Fernández-López A. Post-ischemic salubrinal treatment results in a neuroprotective role in global cerebral ischemia. J Neurochem 2016;138(2):295–306.

